Near Superhydrophobic Carbon Nanotube Coatings Obtained via Electrophoretic Deposition on Low-Alloy Steels

Bruno Alderete,* Timothy MacLucas, Douglas Espin, Sonia P. Brühl, Frank Mücklich, and Sebastian Suarez*

Sucker rods are a key element in certain oil-extraction processes as they link the motor group on the surface with the pumps located downhole. During the transport from the production site toward the extraction well, these components are prone to corrosion. A hydrophobic carbon nanotube (CNT) coating, deposited via electrophoretic deposition (EPD), is proposed as a protective layer, shielding the rods from harsh environmental conditions. Three different coating systems are considered and thoroughly characterized (depending on the additive that is used to deposit the CNT), namely, magnesium nitrate hexahydrate (Mg–Nit), triethylamine (TEA), and a duplex coating (DD). The latter presents an approach which combines the advantages of each additive, mechanical stability from Mg–Nit and strong hydrophobicity from TEA (near superhydrophobic). The former coatings are further processed to overcome their individual shortcomings, resulting in an increase in the coating's stability for TEA coating, as well as transforming the hydrophilic Mg–Nit surface into a hydrophobic surface.

1. Introduction

In the oil-extracting industry, many key components are combined to effectively extract fossil fuels. One of these elements are the sucker rods, which are the links connecting the components on the surface (motor group) and the downhole components (pumps). Due to the chemical composition of the sucker rod's material (low-alloy steel), they suffer from premature corrosion, primarily as a consequence of the saline environment they are subjected to during transport from the production site to the extraction wells. This work proposes a novel approach to counteract the premature corrosion by applying a protective carbon nanotube (CNT) coating on the rods, so as to form a barrier between the steel's surface and the corrosive environment.

Over the past two decades, CNT have been of great interest to the research community due to their outstanding physical properties (mechanical, electrical, thermal, etc.),[1–6] leading to a wide range of promising applications, such as in electrical contacts and bridging, chemical sensors, material coatings, and reinforcements, among others. The major drawback that CNT present is their tendency to form agglomerates as a consequence of π–π interactions (Van der Waals interactions). When agglomerates are formed, the earlier-mentioned properties of the CNT are diminished compared with the intrinsic properties of the individual CNT. In addition to their desirable physical properties, CNT are intrinsically highly hydrophobic particles,[7,8] making them a suitable candidate for surface protection, as shown in a previous study by MacLucas et al.[9]

There are several methods used to deposit CNT (dip coating, drop casting, spin coating, spray coating, etc.).[8,10–17] However, for this study, electrophoretic deposition (EPD) is adopted on account of the advantages it presents,[18–25] namely, modest equipment requirements, easy controllability, cost effectiveness, scalability, and the ability to coat complex geometries. During EPD, an electric field is created between the substrate that will be coated and a counter electrode. Both electrodes are immersed in a colloid consisting of a solvent and the coating material. The electric field between the two electrodes forces the CNT particles to move toward the deposition electrode, which is charged opposite to the surface of the CNT.

B. Alderete, T. MacLucas, Prof. F. Mücklich, Dr. S. Suarez
Chair of Functional Materials
Saarland University
Campus D3.3, Saarbrücken 66123, Germany
E-mail: bruno.alderete@uni-saarland.de

B. Alderete, Prof. S. P. Brühl
Grupo de Ingeniera de Superficies
FRCU
Universidad Tecnologica Nacional
Ing. Pereyra 676, Entre Ríos 3264, Argentina

D. Espin
New Technology Innovations
Science Park 2, Saarbrücken 66123, Germany

Dr. S. Suarez
Universitat des Saarlandes Naturwissenschaftlich-Technische Fakultat
E-mail: s.suarez@mx.uni-saarland.de

Before deposition, the CNT has to be dispersed in a suitable solvent (isopropanol) along with an additive, which improves the colloid's stability and promotes a more homogeneous coating.[9] The additives studied are triethylamine (TEA) and magnesium nitrate hexahydrate (Mg–Nit),[9,26,27] both producing coatings with different characteristics. Previous studies show that coatings produced using TEA result in mechanically unstable, near-superhydrophobic coatings. However Mg–Nit coatings result in hydrophilic and more stable coatings (on account of the formation of a holding layer).[27] To overcome the individual shortcomings of each additive, a double deposition (DD) process is proposed, which consists of an initial Mg–Nit coating on top of which a TEA coating is deposited. In theory, this should result in a strongly hydrophobic coating with enhanced mechanical stability.

Moreover, mechanically breaking up CNT agglomerates improves the dispersion's stability.[9] This is achieved by shear mixing the dispersion, followed by sonication which further breaks down the agglomerates, thus resulting in smaller CNT particles and agglomerates.[28] This is desired as smaller CNT particles, and agglomerates allow the formation of a more homogeneous coating.

To compensate the deficiencies of each of the individual additive, a postprocess is proposed in this work to further enhance the properties of the obtained coatings and modify the surfaces' wetting behavior. This postprocess consists primarily of immersing the coated samples in crude oil, thus filling the porous space of the CNT coating, and placing them in an oven. This step attempts to replicate the conditions in an oil well. No previous study was found discussing the effects of postprocessing (PP) a CNT coating with regard to its wetting behavior.

Within the scope of this work, the structural integrity of the CNT, the coatings' chemical composition, its electrical properties, as well as the wetting behavior of its surface were studied. The surfaces were observed using scattering electron microscopy, and the compactness/pore density of the coatings was observed by milling the coatings with focused ion beam (FIB). The structural integrity was studied via Raman spectroscopy. The chemical composition was analyzed via energy-dispersive X-ray spectra, performing map analysis of the surfaces, as well as line scans. The electrical properties were studied with the four-probe method using direct current (Ohmic relationship), whereas the wetting behavior was studied via sessile drop test. The latter represents the primary focus of this study, as it is an effective method used to assess the efficacy of the coating in regard to corrosion protection.

2. Experimental Section

The metal substrates consisted of a half-cylindrical piece obtained by cutting a cross section of the core region of a sucker rod made of a low-alloy steel (API C grade 1530M), with approximate dimensions of 25 mm base, 15 mm width, and 10 mm height with a 3 mm-diameter screw hole on one of the flat surfaces for holding purposes. The as-received rod's surface was analyzed by confocal laser scanning microscopy (CLSM) LEXT OLS4100 (Olympus) working with a laser wavelength of 405 nm. The measurements were carried out with a 20× objective (N.A. = 0.60). These rods were previously tempered and sandblasted, resulting in a root mean square roughness $S_q = 39.92 \, \mu m$. **Figure 1**a,b shows a laser intensity map of the initial surface to be coated and a topography map of the same region acquired, respectively.

To ensure optimal deposition, both samples and counter electrodes were subjected to a cleaning procedure according to MacLucas et al.,[9] which consisted of three consecutive cycles in an ultrasound bath while being immersed in three different media, namely, cyclohexane, acetone, and isopropanol. Between each step, all samples and counter electrodes were rinsed with deionized water. Finally, the samples were dried with compressed air (4 bar). The cleaning process was kept at 5 min per medium as the steel is prone to unwanted chemical reactions (e.g., oxidation). The coating was applied on the curved surface of the samples using a curved counter electrode to ensure a uniform electric field, as shown schematically in **Figure 2**.

Two suspensions with different additives were prepared consisting of CNT, a suitable solvent (isopropanol), and a dispersing additive (either TEA or Mg–Nit). The chemicals and concentrations used are shown in **Table 1**. The CNT used were chemical vapor deposition (CVD)-grown multiwall CNT (Graphene Supermarket, USA), with an outer diameter distribution between 50 and 85 nm, an as-received state length from 10 to 15 μm, and carbon purity over 94%.
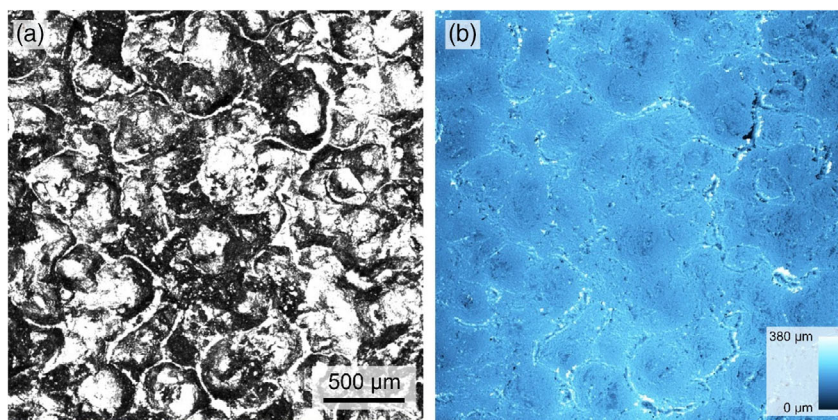

Figure 1. a) Laser intensity map and b) topography map of the sample surface before the coating process, obtained by laser scanning microscopy.
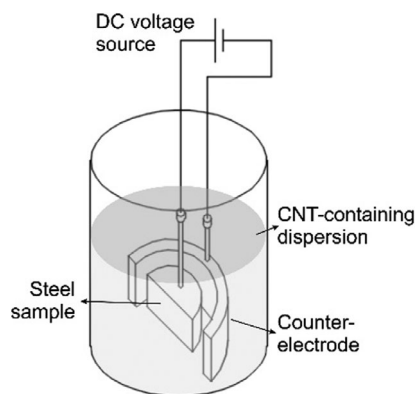
Figure 2. Schematic representation of the EPD setup.

Table 1. Chemicals and concentrations for colloidal preparation.

	TEA coating	Mg–Nit coating
Solvent	80 mL C_3H_8O (Isopropanol)	
Nanoparticle	8 mg CNT	
Additive	10 mL $C_6H_{15}N$ (TEA)	2 mg $Mg(NO_3)_2{\cdot}6H_2O$ (Mg–Nit)
Promoter	–	10 mL Deionized H_2O

Deionized water was added to the Mg–Nit colloid since it was proved by Santhanagopalan et al. that it promotes the formation of a $Mg(OH)_2$ holding layer between the substrate and the coating.[29] To prepare the colloids, the solvent was added, along with the additive, nanoparticles, and deionized water, in the case of Mg–Nit. Subsequently, the colloid was dispersed for 5 min in a shear mixer (IKA T25 digital Ultra-Turrax), followed by 10 min in an ultrasonic bath (Bandelin Sonorex Super RK 514 BH, 33 Hz, 860 W) to homogenize the dispersion. The solution composition used to prepare the colloids was proposed by MacLucas et al.,[9] as well as the preparation process. It is important to highlight that the CNT dispersion tends to coagulate and reform CNT agglomerates. Therefore, a newly dispersed solution was prepared before each deposition process, seeking to immediately conduct the coating's deposition after concluding the dispersion process.

To deposit the CNT onto the steel substrate, the sample was connected to a DC power supply and subsequently immersed in the suspension. The distance between the deposition electrode and the counter electrode was set at 1.5 cm, the voltage at $150 V_{DC}$, and the deposition time varied depending on the additive used, 3 min for the suspension that contained TEA and 5 min for the suspension containing Mg–Nit.

A set of samples were subjected to a DD process utilizing both additives. There, the deposition sequence was 3 min for Mg–Nit and 2 min for TEA. After all depositions, the samples were rinsed in isopropanol. To ensure complete evaporation of any solvent residue, rinsing was followed by 10 min of drying in a ventilated furnace at 80 °C. This is especially important for TEA and DD coatings due to the polar nature of TEA.[9] Improper rinsing of residual TEA will affect the wetting behavior of the coating.

To further optimize the characteristics of the obtained coatings, a PP route is proposed with the aim of improving the coating's wetting behavior and reducing its mechanical instability. This postprocess involved submerging the coated samples in crude oil (Perenco Ltd.) and remaining in an oven at 80 °C for 1–4 days, 1 day for Mg–Nit-based coatings and 4 days for TEA-based coatings. After this process was completed, the samples were removed from the oil and placed once again in the ventilated oven, this time at 200 °C for 4 h, so as to completely dry the samples and remove any excess oil.

Scanning electron microscopy (SEM) analysis was conducted on a dual-beam workstation Helios NanoLab 600 (FEI). The coatings obtained were characterized via energy-dispersive X-ray spectroscopy (EDS) to qualitatively analyze the chemical composition and observe the spatial distribution of the chemical elements throughout the surface of each coating. EDS was conducted at 15 keV with a current of 22 nA and a dwell time set at 200 μs. The final elemental maps consisted of a summation of 16 acquired frames. The structural integrity of the CNT was analyzed by Raman spectroscopy (inVia Raman microscope, Renishaw). The laser wavelength was 532 nm and the measurements were carried out with a $50\times$ objective (N.A. = 0.90), resulting in a spot size of $\approx$5 μm. The spectral resolution was 1.2 cm^{-1}.

The electrical contact resistance (ECR) of the both coatings (Mg–Nit and TEA) was measured, along with a reference measurement of the steel substrate. These measurements were conducted by applying 100 mA of direct current between the sample and a gold-coated rivet ($AuCo_{0.2}$). At the same time, the contact force varied ranging from 0.25 to 4 N with steps of 0.25 N. Two measurements cycles were conducted, where each cycle consisted of a loading phase, followed by an unloading phase. For each force applied, ten measurements were taken. Further specifics about the measurement setup can be found in the study by Puyol et al.[30] Finally, the coating's wetting behavior at room temperature was analyzed by sessile drop testing in a Krüss DSA 100B Drop Contour Analyzer. Deionized water was used to determine the contact angle, with a droplet volume of 3 μL.

3. Results and Discussions

3.1. Morphological Characteristics

The top views of the obtained coatings are shown in **Figure 3** for the Mg–Nit, TEA, and DD samples. As shown in Figure 3a, the surface obtained utilizing Mg–Nit presents some CNT agglomerates and overall good compactness, without evident porosity. The TEA sample's surface (shown in Figure 3b) presents a larger irregular morphology, with extensive regions in which larger CNT agglomerates are recognizable. In this sample type, no porosity could be observed with the magnification chosen.

This is an advantage in terms of corrosion protection, as pores represent a pathway for fluids to infiltrate the coating toward the substrate. In terms of homogeneity, the Mg–Nit samples appear more homogeneous, whereas the TEA coating is less uniform, showing regions with larger CNT agglomerates and others without. Finally, the DD coating (Figure 3c) presents a significantly higher roughness with evident open porosity and agglomerates in a size range comparable with the one observed in the TEA sample. This is a consequence of the surface state between the first (Mg–Nit) and the second (TEA) deposition steps, which
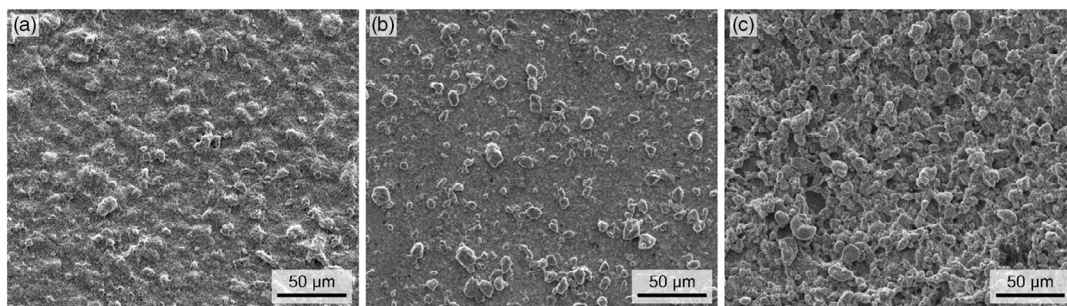
ADVANCED
SCIENCE NEWS
www.advancedsciencenews.com

ADVANCED
ENGINEERING
MATERIALS
www.aem-journal.com

Figure 3. Top view of the scanning electron micrographs of the coatings: a) Mg–Nit, b) TEA, and c) DD.
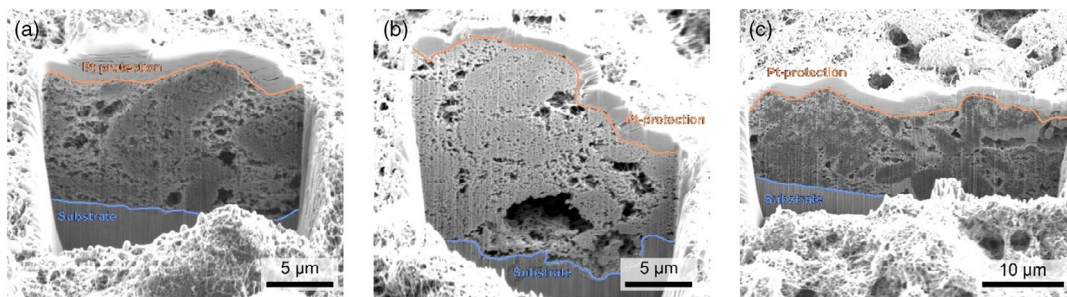

Figure 4. FIB cross sections of the coatings: a) Mg–Nit, b) TEA, and c) DD.

provides an irregular surface to the CNT being deposited in the TEA step. These irregularities have a dual effect on the final roughness. First, the Mg–Nit coating will copy the substrate and enhance the irregularities. Second, the outstanding agglomerates might act as sites with enhanced electrical field intensity (due to their local curvature), increasing the deposition rate at those specific sites, resulting in an inhomogeneous CNT distribution.

Figure 4 shows the cross sections of the coatings obtained by FIB milling. Regarding the coatings' compactness, the micrographs present a different picture from what could be inferred from the top view. The Mg–Nit and the DD coatings (Figure 3a,c, respectively) show an acceptable compactness, with some scattered pores in the µm range and irregular shape. On the other hand, the TEA coating (Figure 3b) shows more pores in the aforementioned size range and a larger one close to the substrate interface, having a diameter of ≈5 µm. These kinds of voids in that position might compromise the proper adherence of the coating to the steel substrate. Focusing specifically on the coating–substrate interfacial features of the analyzed samples, besides the previously mentioned TEA sample, both the Mg–Nit and the DD show a quite seamless interface to the steel substrate. This is a consequence of the formation of the $Mg(OH)_2$ holding layer, that enhances the adhesion and promotes the compact growth of the CNT coating, as shown in previous reports.[9] The mean thickness measured from these images was Mg–Nit (12.5 ± 0.9) µm, TEA (16.2 ± 4.7) µm, and DD (14.4 ± 0.9) µm. The strong variation in thickness from the TEA sample is associated with large pores observable at the interface with the substrate, resulting in a more irregular profile. It seems that the use of Mg–Nit as an additive for the production of the coating as standalone or as a bottom layer for a subsequent coating positively influences the thickness homogeneity, the coating's

compactness, and the interface to the substrate. It is important to highlight that the thicknesses measured for the set of coatings contrast the results obtained by MacLucas et al.[9] In their study, using Mg–Nit as an additive resulted in thicker coatings, and using TEA resulted in thinner coatings, for comparable deposition times. As shown before, here TEA results in a thicker coating. This may be a consequence of the holding layer that is formed during the deposition process of Mg–Nit coating. The holding layer smoothens the surface of the substrate, slowing down the deposition rate of CNT. Given that there is no holding layer on TEA samples, the asperities of the substrate potentially enhance the local electric field, producing a thicker, and less uniform, coating over these asperities.

To understand the structural state of the CNT after the coating process, Raman characterization is made of each sample (**Figure 5**). The focus is placed on tracing the change in the typical defect index, which relates the intensities of the D and G band (I_D/I_G).[31] The resulting values of the ratio are pristine CNT: 0.71, Mg–Nit: 1.06, and TEA: 0.64. The difference between the TEA sample and the pristine CNT is marginal, both values within the normal range, highlighting that this additive does not affect the structural state of the CNT after deposition. On the other hand, the increased value for the Mg–Nit sample could be associated with both, the attachment of chemical species and the formation of the holding layer during the deposition process.

3.2. Chemical Composition

EDS spectra were acquired to investigate the chemical characteristics of the different coatings, as shown in **Figure 6**. For the three cases studied, the main chemical elements detected are
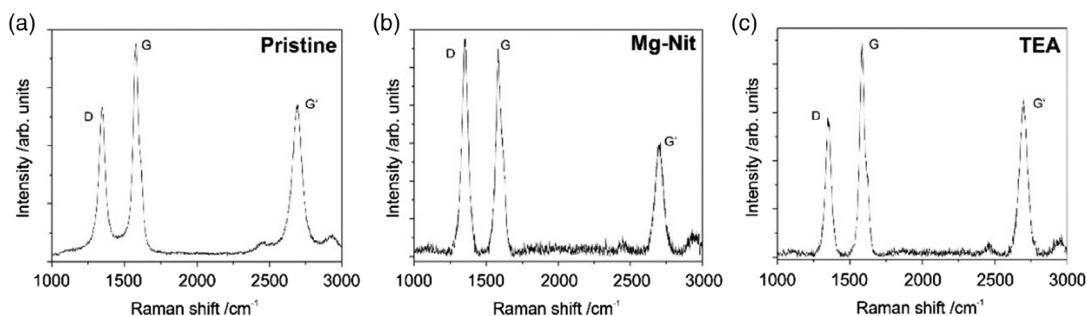
Figure 5. Raman spectroscopy: a) pristine CNT, b) TEA sample, and c) Mg–Nit sample.
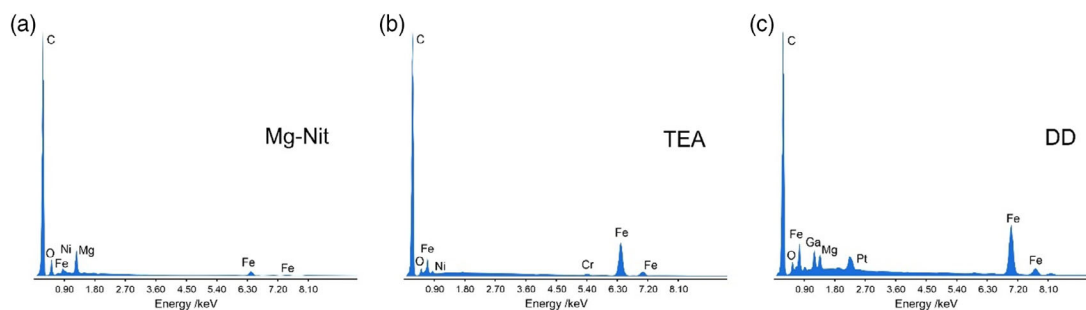

Figure 6. EDS spectra of the a) Mg–Nit, b) TEA, and c) DD coatings.

carbon, magnesium (only when Mg–Nit was used as an additive, Figure 6a), oxygen, nickel, and iron. Clearly, the detected carbon stems from the CNT. The detected oxygen for Mg–Nit coatings has different origins, being mainly from the carboxy groups present in the CNT as a consequence of CVD synthesis, the $Mg(OH)_2$ holding layer in the Mg–Nit sample, and, to a minor extent, from light oxidation found on the surface of the substrate after the cleaning process.

This becomes more evident when analyzing the elemental distribution maps shown in **Figure 7**. Here, it is observed that both the Mg–Nit and the DD coatings have a more homogeneous carbon distribution than TEA coating (Figure 7, second row). Consequently, these results agree with the previous observations (Figure 3), that the TEA sample is less homogeneous than the Mg–Nit sample. The variation in this coating's thickness (TEA) is a consequence of the higher quantity of CNT agglomerates that are present during the deposition process, as this additive promotes the formation of particle agglomerates. The oxygen map shown in Figure 7 also supports this observation, proving that the coating thickness varies significantly from region to region, showing weaker intensity where the carbon intensity peaks and showing stronger oxygen intensities where carbon concentrations are lower. It can be deduced that the oxygen content detected by EDS for TEA is primarily due to the oxidation present on the sample's surface and has negligible influence from the carboxy groups bonded to the CNT, as oxygen is detected in higher amounts where the coating appears thinner. In addition, as depositing CNT with TEA does not produce chemical reactions (e.g., formation of a holding layer), it is understood that oxygen is not retained by any dissociating ions. On the other hand, the Mg–Nit coating shows a homogenous oxygen distribution, which might be associated with the holding layer and the retention of oxygen in

combination with Mg^{2+} ions after the dissociation of the additive precursor, as well as the nitride ions. Finally, the DD coating shows a very low oxygen concentration, in agreement to what has been observed on the TEA coating. This oxygen distribution is, as already mentioned, likely from surface oxidation of the steel substrate. For DD coatings, oxygen is not observed uniformly like in Mg–Nit given that EDS shows relative intensities.

To further understand how the elemental composition of the coating varies as it is deposited, EDS depth compositional profile analysis along FIB cross section was conducted, results are shown in **Figure 8**. In this figure, the blue arrow indicates the scan direction, from the substrate's surface upward toward the coating's surface. The FIB cross section additionally shows the porous network of the CNT coating. As shown, the lower Mg–Nit region possesses several large pores, whereas the upper TEA coating contains smaller but more abundant porosity. The dashed line highlights the interface between both coating steps.

For this analysis, the elements of interest are carbon, oxygen, and magnesium. As expected, carbon is found throughout the entire coating with some variations. The oxygen content along the same trajectory is highest close to the substrate, and rapidly decreases, remaining fairly constant as the scan progresses. This effectively proves that the vast majority of the oxygen detected in the EDS maps for the DD coating is due to the substrate's oxidation, and a small amount is detected from the functionalization of the CNT (carboxy groups). However, there is a region with increased oxygen and magnesium concentration between 1 and 2.5 µm away from the substrate (highlighted in grey in the concentration profile). This is associated with the $Mg(OH)_2$ holding layer, which forms between the coating and the substrate. Thereafter, a continuous decrease in magnesium is observed as the scan progresses toward the TEA region.
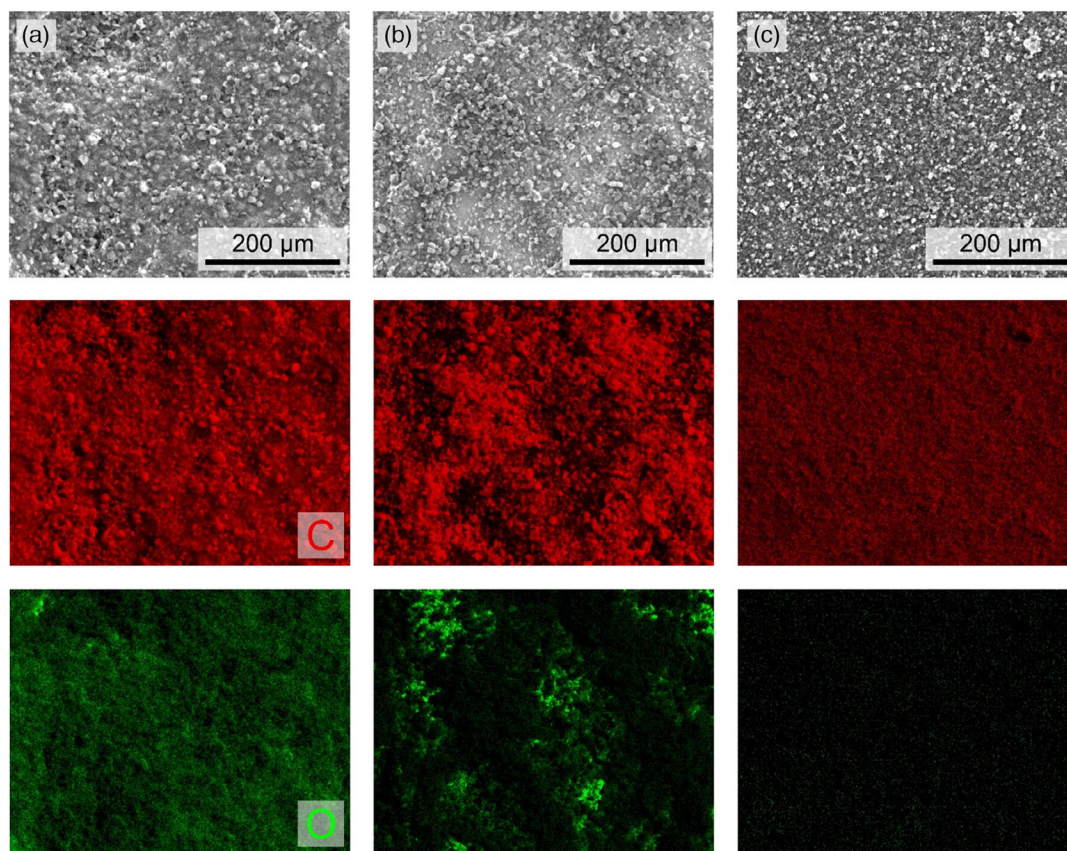
**ADVANCED
SCIENCE NEWS**
www.advancedsciencenews.com

*ADVANCED
ENGINEERING
MATERIALS*
www.aem-journal.com

Figure 7. Elemental concentration maps for the a) Mg–Nit, b) TEA, and c) DD coatings. The first row depicts the secondary electrons micrographs, the second and third row correspond to the carbon and oxygen maps, respectively.
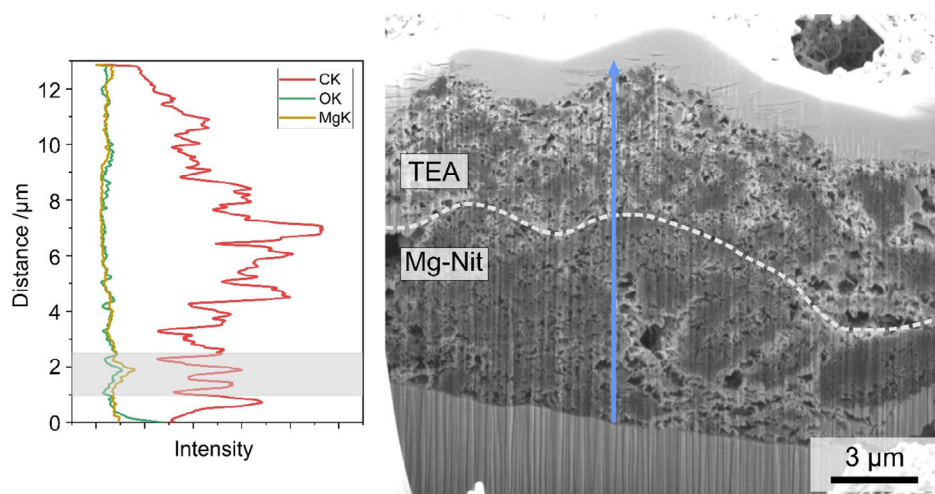

Figure 8. FIB cross section of the DD sample with linear trajectory for chemical analysis.

3.3. Coating Characterization after PP

As explained in the experimental part, the coatings were subjected to a PP treatment in crude oil at 80 °C, so as to investigate changes in the coating structure and chemistry that might occur under operating conditions in an oil well. **Figure 9**a,c shows the chemical spectra of the Mg–Nit and TEA postprocessed samples, respectively. After the treatment, the chemical analysis shows sulfur in both coatings, however, in very low concentration for the TEA sample, whereas untreated samples did not show sulfur
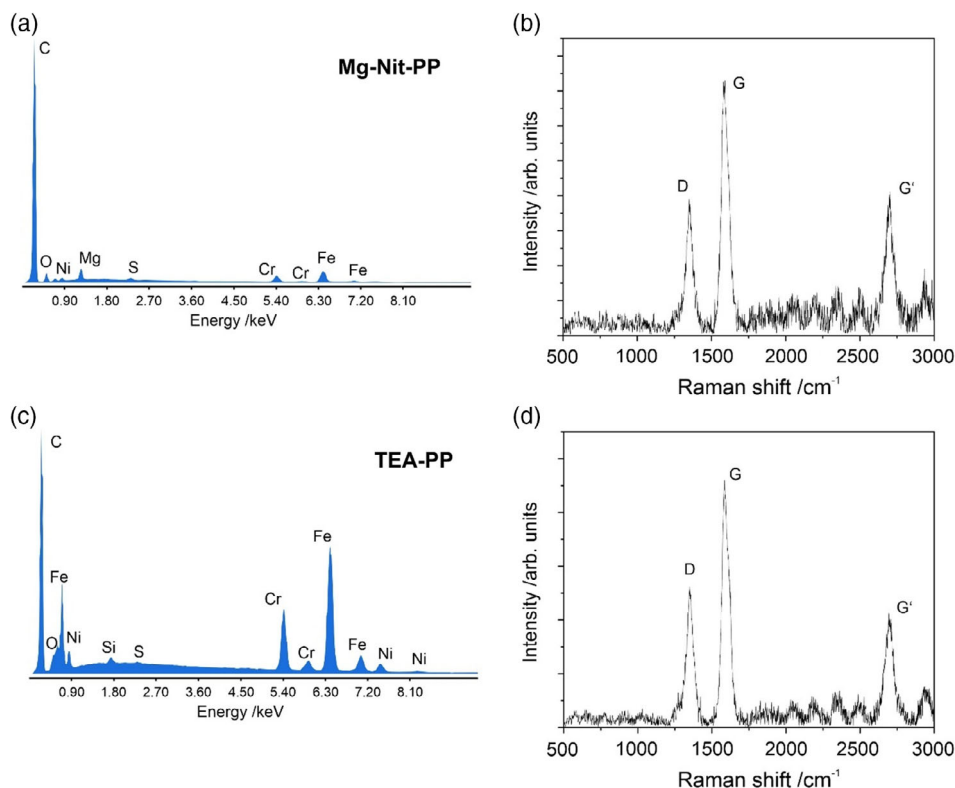
2001448 (6 of 11)

Figure 9. a) EDS and b) Raman spectrum of the postprocessed Mg–Nit coatings. c) EDS and d) Raman spectrum of the postprocessed TEA coatings.

in any of the measurements. Hence, it is reasonable to assume that it stems from the interaction between the crude oil and the coating. This indicates that during PP, the crude oil was able to infiltrate the coating and that it reacted with the species present in the coating. This observation is supported by the fact that hydrocarbons tend to show good wetting compatibility with carbonaceous coatings (oleophilic). For the Mg–Nit coating in particular, any remaining Mg would form ionic bonds with S molecule, transforming the Mg molecules into magnesium cations Mg^{2+} and the S molecule into sulfide anions S^{2-}, completing outer-electron configuration (octet). The ionic bond produces magnesium sulfide ($Mg^{2+} + S^{2-} \rightarrow MgS$). In addition, given the presence of water (promoter) and carboxy groups in the Mg–Nit coatings, S could also react with Mg to form magnesium sulfate ($Mg^{2+} + SO_4^{2-} \rightarrow MgSO_4$). The formation of one, or both, of these compounds does not cause the surface's behavioral transformation, but the behavioral properties of these compounds allow the inference of which compound is primarily formed. Given that magnesium sulfide is hydrophobic, it is expected that the magnesium ions predominantly react with sulfur to form magnesium sulfate.

Finally, Figure 9b,d shows the Raman spectra of the coatings after the crude oil treatment. Structurally, the Raman indicators show marginal improvements in I_D/I_G after oil processing, when compared with the values shown in the previous section (Mg–Nit-PP: 0.53 and TEA-PP: 0.57). Although both values are within the normal range, this change may be related to minimal graphitization of the sample and thermal degradation into graphitic carbon of the oil.

3.4. Electrical Properties

The average resistance as a function of the applied force is shown in **Figure 10**, with a shading differentiation for each measurement semicycle (loading and unloading). As shown, the steel substrate presents the lowest contact resistance, beginning at around $1.4\,\Omega$ and stabilizing at around $0.2\,\Omega$ after the first measurement semicycle concludes. The Mg–Nit sample presents the highest initial contact resistance at 0.25 N but rapidly decreases as the normal force increases. Near the end of the first semicycle (3.75 N), the resistance reached its stabilized value of $\approx 1.3\,\Omega$, which corresponds to the highest value measured for the steel substrate. The TEA coating presents the lower variation from the beginning of the measurement until the end, when compared with the Mg–Nit coating and the substrate. However, it presents the highest resistance overall, with an initial value of over $70\,\Omega$ and stabilizing at $\approx 30\,\Omega$.

As previously mentioned, the Mg–Nit coating presents CNT agglomerates and a higher density of pores than the TEA coating. This may explain the high initial resistance of the Mg–Nit coating, along with the sharp decrease as the applied force increases. When the force increases, the cavities are closed and CNT agglomerates are displaced by the counter electrode, reducing the voids within the coating, giving way for the current to flow through the coating and toward the substrate. As the Mg–Nit coating is compacted by the counter electrode, the resistance drops from nearly $130\,\Omega$, down to a stabilized value of $\approx 1.3\,\Omega$. In the TEA coating, on the other hand, the compressing effect of the counter electrode is less significant given that the
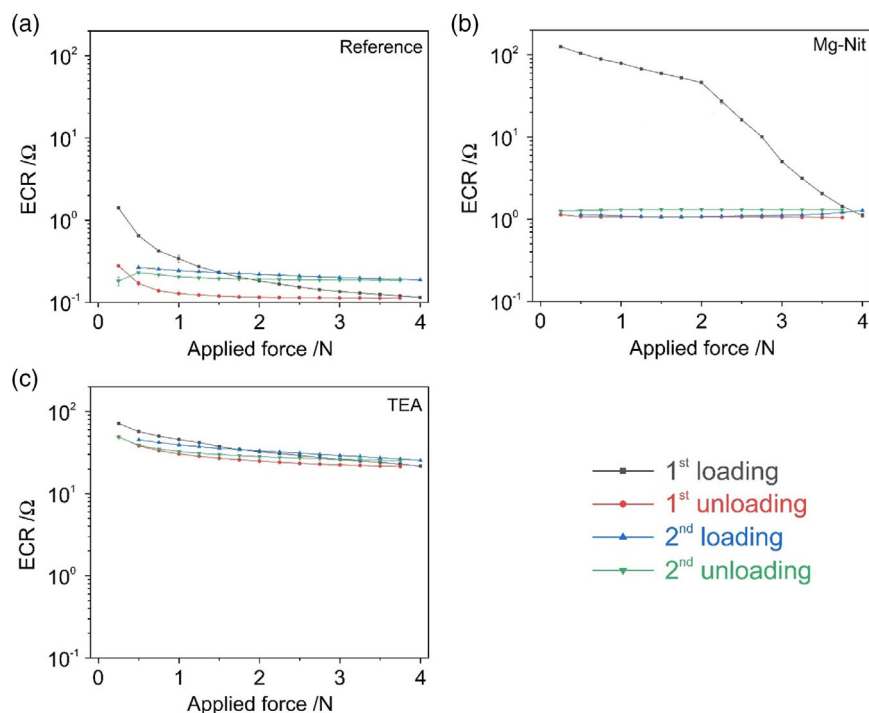
Figure 10. ECR current sweep of a) a steel substrate, b) Mg–Nit, and c) TEA.

distance between CNT particles before applying the force is lower than the Mg–Nit coating. When the counter electrode begins to compress the coating, the CNT coating begins to be displaced and gradually fills some of the smaller pores. However, given the number of pores within the coating, the ones that are compacted are insignificant. This porous network may be the reason for the high resistance of the TEA coating for light loads (70 Ω) but also the elevated stabilization resistance (30 Ω). The reference sample shows a typical metal–metal contact behavior, with low contact resistance, whereas the coatings are dominated by the typical high contact resistance of CNT agglomerates. However, Mg–Nit shows after the first semicycle a transition to a metal–metal contact that remains as a permanent feature. This is likely a consequence of the interaction between the coating and its holding layer, which renders the coating prone to permanent deformation. This is not the case for the TEA coating, which shows almost complete elastic restitution, given by the very similar loading and unloading response. This is defined by the strain rate-independent destruction and formation of van der Waals interactions in CNT agglomerates.[32,33] From a mechanical point of view, the TEA coating would protect the surface in a more efficient way, in a wider range of normal loads than the Mg–Nit coating.

When considering only the electrical characteristics of the coating, the Mg–Nit coating comes out as the better conductive of both. Although the initial resistance is higher than the TEA coating, after 3.75 N, the resistance is less than one order of magnitude higher (1.3 Ω) than that of the steel substrate's stable resistance (0.2 Ω). Given that the main objective of this coating is to protect the substrate from harsh environments, this slight gain in electrical resistance is a favorable tradeoff.

3.5. Wetting Behavior

The wetting behavior of all coatings was compared with that of an uncoated steel reference and the images used for the analysis are shown in **Figure 11**. **Table 2** shows the contact angle measurements obtained for the different surfaces.

For the as-deposited Mg–Nit coating, an average contact angle of 34.6° was measured. This was within the expected values, as it was reported by MacLucas et al. that as-deposited Mg–Nit coatings result in a hydrophilic surface.[9] This hydrophilic surface is a result of the interactions between the water droplet and the magnesium ions that are formed during the deposition process itself. Nonetheless, after the postprocess, the Mg–Nit surfaces are transformed from a hydrophilic surface to a near-superhydrophobic surface (superhydrophobic surface >150° in contact angle) with an average contact angle of 144.9°. This transformation assimilates to a surface that is over three times more hydrophobic, compared with the untreated Mg–Nit coating (34.6°). The transformation from a hydrophilic to a hydrophobic surface may be explained by molecular sulfur found in the postprocessed coating.[34] Another possible explanation for this transformation is that the Mg^{2+} ions form magnesium sulfide. Therefore, the coating is depleted of free magnesium ions and the water droplets no longer interact with the coating. Moreover, the magnesium sulfide that is formed is hydrophobic, further promoting a hydrophobic behavior. In addition, it was empirically discovered that for the Mg–Nit coating, the determining parameter to improve the surface's wetting behavior is coating's thickness (up to 5 min deposition time).

PP for longer periods of time does not significantly improve the surface's wetting behavior (as shown in **Table 3**). Varying the
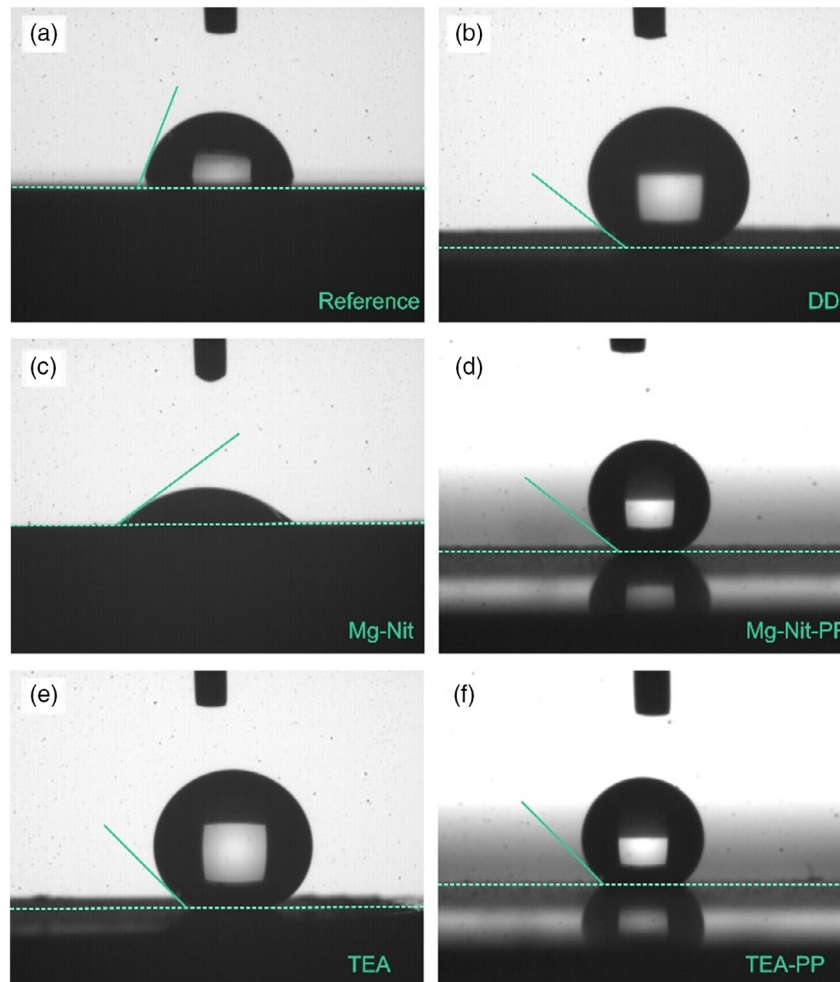
Figure 11. Images acquired to analyze the wetting behavior of a) Reference, b) DD, c) Mg–Nit, d) postprocessed Mg-Nit, e) TEA, and f) postprocessed TEA. The green dashed line indicates the object baseline and the green solid line, the tangent to the deposited droplet.

Table 2. Contact angle measurements for the different surfaces.

Sample	Reference	DD	Mg–Nit	Mg–Nit–PP	TEA	TEA–PP
Contact angle [°]	74.2 ± 4.4	140.5 ± 4.0	34.6 ± 6.0	144.9 ± 1.3	139.5 ± 4.0	136.9 ± 1.6

Table 3. Determining parameter for postprocess. Thickness (higher deposition times) is key in Mg–Nit samples, whereas prolonged PP time is key for TEA samples.

Deposition and postprocess time for each sample type				
Sample	Mg–Nit	Mg–Nit	TEA	TEA
Deposition time [min]	2	5	2	2
Postprocess time [days]	1	1	2	4
Average contact angle [°]	116.3	144.9	115.1	136.9

coating's thickness, however, does vary the contact angle measurements obtained. Although the postprocess time does not significantly influence the result, it is important to highlight that the process is essential, due to the fact that without this process the surface attained is hydrophilic.

Contrary to Mg–Nit, the TEA sample shows a near-superhydrophobic wetting behavior with an average contact angle of 139.5°. After the postprocess, the TEA samples' average contact angle remains somewhat similar, with a slight decrease to 137°. Although the contact angles of the postprocessed TEA samples are lower than the untreated TEA samples, the postprocessed surfaces are more mechanically stable. Obtaining a more robust coating is strongly desired. Hydrophobicity is not an effective protective mechanism if the coating is easily removed by scratches, vibrations, or impacts. Therefore, the negligible loss in hydrophobicity is within a certain tolerance given the reduction in the coating's instability. Moreover, for TEA samples, the determining parameter in the postprocess is the process time

(Table 3). In contrast to the Mg–Nit samples, postprocessed TEA coatings don't require prolonged deposition times (from 2 to 3 min deposition times). It is however required that the coating covers the entire surface, but in regard to thickness, there is no specific requisite. For shorter postprocess times, the coating's stability is increased, improving sample manipulation. Two identically deposited coatings were compared, one of which was postprocessed for 2 days, the other for 4 days. The sample that was postprocessed for 2 days presents enhanced mechanical stability at the cost of ≈21° in contact angle on average. The coating that was postprocessed for 4 days, however, also presents the enhancement of mechanical stability, with an average contact angle drop of only 2°. Therefore, it can be stated that the determining parameter for the postprocess is the process time. With an increase in postprocess time, the sample's mechanical stability also increases, whereas the loss in contact angle is, to some degree, negligible.

The wetting behavior of the DD sample is similar to that of the TEA surface with values of 140.5°. This was to be expected as the surface of the DD sample is a CNT coating that uses TEA as an additive. This additive produces a strong hydrophobic surface (near superhydrophobic), over the existing Mg–Nit coating. Therefore, DD samples show increased coating stability as a consequence of the holding layer that is formed during the Mg–Nit deposition, in addition to near superhydrophobic surface on account of the superficial TEA coating. Based on these results, this system represents a promising solution for the chemical protection of the surface. Furthermore, this coating system is viable without the need of the additional postprocess.

The presence of sulfur is the only difference observed between the samples that have been postprocessed and the ones that have not, the enhancement in terms of wetting behavior is attributed to this element and its interactions with the coating and/or substrate. The extensive drying procedure (4 h at 200 °C) conducted after the postprocess aims at leaving no crude oil remains trapped within the porous matrix of the coatings; however, some long hydrocarbon chains might remain within its thickness. As a consequence of the fluid's hydrophobic nature, it would explain the gain in the coating's hydrophobicity. The introduction of sulfur into the coating further increases the hydrophobic behavior of the coating due to the hydrophobic nature of molecular sulfur,[34] along with the depletion of Mg^{2+} ions and formation of magnesium sulfide, in the case of Mg–Nit–PP samples.

4. Conclusion

The behavioral properties and characteristics of three different coating systems (Mg–Nit, TEA, and DD) have been studied, as well as a novel postprocess, consisting of the thermal treatment of the coating submerged in crude oil at 80 °C (PP). Mg–Nit coatings present good compactness, are highly homogeneous with scattered pores in the μm range, and possess a seamless interface with the substrate. These coatings present high electrical resistance (130 Ω), that stabilizes at 1.3 Ω. In terms of wetting behavior, they present a mechanically stable, hydrophilic surface (34.6°). After PP, Mg–Nit coating's surface becomes near superhydrophobic (144.9°), while maintaining mechanical stability. TEA coatings present irregular morphology with scattered

CNT agglomerates and μm range pores and 5 μm pores near the interface. The coating shows elastic restitution, with elevated electric resistance (30 Ω stable resistance). The coating is near superhydrophobic without the PP (139.5°) but mechanically unstable. After PP, TEA coatings retain their near superhydrophobicity, while presenting an increased stability. Finally, DD coatings share characteristics from both coatings. Morphology and compactness are comparable with Mg–Nit coatings (compact, scattered pores, seamless interface), with near super-hydrophobic surface similar to non-PP TEA coatings (140.5°). This validates the hypothesis that DD coatings could overcome the individual shortcomings of each additive, potentially protecting the substrate from corrosive environments.

Considering the conditions in which the sucker rods are transported and subjected to once in operation, it would be of interest in future studies to analyze more precisely the corrosion protection that the coatings provide, using different techniques like salt spray fog tests, electrochemical impedance spectroscopy, and potentiodynamic tests in different media.

Conflict of Interest

The authors declare no conflict of interest.

Data Availability Statement

Research data are not shared.

[1] M. A. Meyers, A. Mishra, D. J. Benson, *Prog. Mater. Sci.* **2006**, *51*, 427.

[2] P. Kim, L. Shi, A. Majumdar, P. L. McEuen, *Phys. Rev. Lett.* **2001**, *87*, 215502.

[3] S. Nasir, M. Z. Hussein, Z. Zainal, N. A. Yusof, *Materials* **2018**, *11*, 295.

[4] P. Ajayan, O. Zhou, in *Carbon Nanotubes* (Eds: M. S. Dresselhaus, G. Dresselhaus, Ph. Avouris), Vol. *80*, Springer-Verlag, Berlin, Heidelberg, Germany **2001**.

[5] S. Beg, M. Rizwan, A. M. Sheikh, M. S. Hasnain, K. Anwer, K. Kohli, *J. Pharm. Pharmacol.* **2011**, *63*, 141.

[6] R. Saito, G. Dresselhaus, M. S. Dresselhaus, *Physical Properties of Carbon Nanotubes*, Imperial College Press, London **1998**.

[7] N. Saifuddin, A. Z. Raziah, A. R. Junizah, *J. Chem.* **2013**, *2013*, 678815.

[8] D. Łukawski, A. Lekawa-Raus, F. Lisiecki, K. Koziol, A. Dudkowiak, *Prog. Org. Coat.* **2018**, *125*, 23.

[9] T. MacLucas, S. Schütz, S. Suarez, F. Mücklich, *Surf. Topogr. Metrol. Prop.* **2018**, *6*, 014005.

[10] C. J. Brinker, in *Chemical Solution Deposition of Functional Oxide Thin Films* (Eds: T. Schneller, R. Waser, M. Kosec, D. Payne), Springer, New York, USA **2013**, Ch. 3.

[11] J. Puetz, M. A. Aegerter, in *Sol-Gel Technologies for Glass Producers and Users* (Eds: M. A. Aegerts, M. Mennig), Springer, New York, USA **2004**, Ch. 2.

[12] K. Kalantar-Zadeh, B. Fry, *Nanotechnology-Enabled Sensors*, Springer, New York, USA **2008**.

[13] N. Sahu, B. Parija, S. Panigrahi, *Indian J. Phys.* **2009**, *83*, 493.

[14] J. F. Taylor, *Met. Finish.* **2001**, *99*, 16.

[15] L. E. Scriven, *Mater. Res. Soc. Symp. Proc.* **1988**, *121*, 717.

[16] R. C. Tucker, *Surface Engineering ASM Handbook* (Eds: C. M. Cotell, J. A. Spargue, F. A. Smidt), Vol. *5*, ASM International, Materials Park, OH, USA **1994**.

[17] M. F. Smith, in *Comparing Cold Spray with Thermal Spray Coating Technologies* (Ed: V. K. Champagne), Woodhead Publishing in Materials **2007**, Ch. 3.

[18] A. R. Boccaccini, J. Cho, J. A. Roether, B. J. C. Thomas, E. Jane Minay, M. S. P. Shaffer, *Carbon* **2006**, *44*, 3149.

[19] J. H. Dickerson, A. R. Boccaccini, *Electrophoretic Deposition of Nanomaterials*, Spinger, New York, USA **2011**.

[20] P. Sarkar, P. S. Nicholson, *J. Am. Ceram. Soc.* **1996**, *79*, 1987.

[21] H. C. Hamaker, *Trans. Faraday Soc.* **1940**, *35*, 186.

[22] M. Farrokhi-Rad, T. Shahrabi, *J. Am. Ceram. Soc.* **2012**, *95*, 3434.

[23] M. Atiq Ur Rehman, Q. Chen, A. Braem, M. S. P. Shaffer, A. R. Boccaccini, *Int. Mater. Rev.* **2020**, 1, https://doi.org/10.1080/09506608.2020.1831299.

[24] Y. Ma, J. Han, M. Wang, X. Chen, S. Jia, *J. Mater.* **2018**, *4*, 108.

[25] L. Li, W. Liu, L. Yang, W. Jiao, L. Hao, R. Wang, *Compos. Sci. Technol.* **2020**, *187*, 107946.

[26] M. F. De Riccardis, D. Carbone, A. Rizzo, *J. Colloid Interface Sci.* **2007**, *307*, 109.

[27] S. Santhanagopalan, F. Teng, D. D. Meng, *Langmuir* **2011**, *27*, 561.

[28] L. Reinert, M. Zeiger, S. Suarez, V. Presser, F. Mücklich, *R. Soc. Chem. Adv.* **2015**, *5*, 95149.

[29] S. Santhanagopalan, A. Balram, E. Lucas, F. Marcano, D. D. Meng, *Key Eng. Mater.* **2012**, *507*, 67.

[30] R. Puyol, S. Suarez, in *IEEE URUCON Montevideo*, IEEE, Montevideo, Uruguay **2017**, pp. 1–4.

[31] S. Suarez, F. Lasserre, O. Prat, F. Mücklich, *Phys. Status Solidi Appl. Mater. Sci.* **2014**, *211*, 1555.

[32] X. Yang, P. He, H. Gao, *Nano Res.* **2011**, *4*, 1191.

[33] J. R. Raney, F. Fraternali, C. Daraio, *Nanotechnology* **2013**, *24*, 255707.

[34] G. W. Walker, C. P. Walters, P. E. Richardson, *Int. J. Miner. Process.* **1986**, *18*, 119.